

## EFFECTIVE STRESS LAWS FOR PETROPHYSICAL ROCK PROPERTIES

John L. Shafer, *Reservoir Management Group*  
Greg N. Boitnott, *NER Inc.*  
Russell T. Ewy, *Chevron*

Copyright 2008, held jointly by the Society of Petrophysicists and Well Log Analysts (SPWLA) and the submitting authors.

This paper was prepared for presentation at the SPWLA 49<sup>th</sup> Annual Logging Symposium held in Edinburgh, Scotland, May 25-28, 2008.

---

### ABSTRACT

Effective stress laws and their application are not new, but are often overlooked or mis-applied. As we observe in deepwater GoM Lower Tertiary (LT) sands, the effective stress coefficient deviates significantly from one and can be quite different for different rock properties of interest.

As petrophysicists, log and core analysts, we need to be aware that pore pressure can have a significant impact on reservoir properties in ways not easily described using a simple effective stress law. These effects must be taken into account when applying measurements made in the laboratory for calibration of reservoir engineering models and calculation of rock mechanical properties from acoustic logs.

An effective stress law is a means to convert two variables, external stress ( $\sigma$ ) and pore pressure ( $P_p$ ), into one equivalent variable ( $\sigma_{\text{effective}}$ ). One such expression would be  $\sigma_{\text{effective}} = \sigma - a P_p$ , where  $a$  is the "effective stress coefficient".

Every rock property; e.g. permeability, compressibility, and acoustic velocities, has its own effective stress coefficient. This coefficient is found to be less than 1.0 for many rock properties, is commonly thought to be 1.0 for strength and static elastic constants, and can be greater than 1.0 for permeability. Typically, the magnitude of the effective stress coefficient is dependent on the stiffness of the rock. Rocks having higher bulk compressibility tend to be characterized by effective stress coefficients closer to a value of 1.0 for a wider range of properties. However, when one combines stiff rock with very high pore pressures, as we observe in LT sands, the effective stress coefficients for many properties can be quite different from 1.0, and can be variable for different properties of interest.

The effective stress coefficient for bulk volume compressibility, the Biot Coefficient  $\alpha$ , is probably the most recognized. Often we find that it is substituted for the effective stress coefficient in effective stress laws for other rock properties such as S and P velocities. We will show that in many cases this may not be appropriate, and can lead to erroneous estimates of in-situ stress, pore pressure, wellbore stability, and permeability.

### INTRODUCTION

The intent of this paper is to draw attention to the potential impact of very high pore pressures on petrophysical measurements and interpretations. For the Lower Tertiary Paleogene play in the ultra deep water (water depths > 5,000 feet) Gulf of Mexico, the wells are drilled to depths in excess of 25,000 feet (7620m). Some wells have set near depth records of about 33,000ft (TVD). Pore pressures can exceed 20,000 psia (138MPa). These wells are very expensive to drill and complete, with costs up to about \$100 million per well. Production scenarios require large pore pressure depletions. Thus it is very important to quantify rock strength, pore compressibility, and changes in permeability during large pore pressure depletions.

The very high pore pressures in the Lower Tertiary Paleogene of the ultra deep water Gulf of Mexico cause unique challenges for rock and fluid property measurements. Routine core measurements used to calibrate logs and constrain reservoir simulations are commonly made at low pore pressures. To mimic reservoir conditions, the tests are performed at reduced external stresses, so as to compensate for the low pore pressures. It is common practice to choose a net effective stress that is thought to result in identical rock properties. In this paper we will discuss the calculation of net effective stress for compaction, permeability, and S and P elastic wave velocities. We will show that due to a variety of pore pressure phenomena, the net effective stress for each property is different. This is true even for a material that behaves as a linear poroelastic material, and is a direct result of the fact that pore pressure and external stresses act in different ways via fundamentally different deformations. This

leads to the conclusion that the “effective stress” should not be thought of as an equivalent state of stress, but rather as a means to relate different states of stress that lead to similar properties. It also points out that one must be very careful in applying core analysis data through models that properly account for a potentially wide variety of pore pressure effects. Failure to do so can lead to potentially significant errors. For example, laboratory measurement of brine permeability as a function of confining stress and pore pressures indicate that for these LT rocks, the routine core permeability measurements at close to zero pore pressure may underestimate the in-situ rock permeability by 20% to 50%.

### EFFECTIVE STRESS LAWS FOR RESERVOIR DEPLETION

One general application where effective stress issues become important is in modeling the effects of pore pressure depletion on compaction and the resulting compaction induced changes in reservoir properties. It is commonly assumed that during pore pressure depletion in a reservoir, the matrix deforms such that the lateral strain remains constant. In geomechanics testing, this loading path is referred to as uniaxial strain.

Uniaxial strain during pore pressure depletion is a rather complicated test to perform and analyze. It is not uncommon for geomechanics testing to be performed at constant pore pressure. In this case pore pressure depletion is simulated by increasing axial stress at fixed pore pressure while maintaining radial strain constant (e.g. no change in radial strain). In designing such tests, the concept of simple effective stress is commonly evoked, e.g. by assuming that an increase in  $\sigma_a$  at constant  $P_p$  (pore pressure) and constant radial strain is equivalent to a decrease in  $P_p$  at constant  $\sigma_a$  and constant radial strain.

While this is true under some limited conditions (e.g. linear poroelasticity with incompressible grains), it is dangerous to assume this equivalence for the particular case of many deepwater GOM sands of interest. It is also erroneous to assume that the two loading paths can be made equivalent through the concept of an effective stress coefficient (e.g. by replacing all external stresses  $\sigma$  with  $\sigma - \alpha P_p$ ).

To illustrate some points, let us first examine the case of linear poroelasticity. This problem was studied in detail in the classic works of Biot [1956,1962] and others, and leads to the now familiar effective stress law for hydrostatic volume compressibility, equation (1).

$$\epsilon_v = P_e / K_b ; P_e = P_c - \alpha P_p ; \alpha = 1 - K_b/K_g \quad (1)$$

where  $\epsilon_v$  is the volumetric strain,  $P_e$  is the effective pressure,  $K_b$  is the bulk modulus of the rock, and  $K_g$  is the bulk modulus of the solid grains. The parameter  $\alpha$  is commonly referred to as the effective stress coefficient. The temptation is to assume that the “effective pressure”  $P_e$  defines an equivalent stress that, when applied to a rock in the absence of pore pressure, results in an equivalent physical state (thus removing pore pressure as a variable). In fact however,  $P_e$  is little more than a functional relationship between  $P_c$  and  $P_p$  that yields identical bulk volume for the case of an isotropic, linear elastic, porous solid.

To illustrate some issues in applying the concept of effective stress to reservoir studies, it is helpful to begin by analyzing the predictions of linear poroelasticity for axi-symmetric loading:

$$\epsilon_a = [(\sigma_a - P_p) - 2\nu(\sigma_r - P_p)]/E + P_p/(3K_g) \quad (2)$$

$$\epsilon_r = [(\sigma_r - P_p) - \nu(\sigma_a + \sigma_r - 2P_p)]/E + P_p/(3K_g) \quad (3)$$

where  $\epsilon_a$  is the axial strain,  $\epsilon_r$  is the radial strain,  $\sigma_a$  is the external axial stress,  $\sigma_r$  is the external radial (confining) stress, and  $P_p$  is the pore pressure. For the case of a homogeneous isotropic poroelastic solid, the material is characterized by 3 elastic constants: two bulk elastic constants ( $E$  and  $\nu$ ) and the bulk modulus of the solid grains ( $K_g$ ). Let us now compare the pore pressure depletion and constant pressure uniaxial strain load paths discussed previously. For the case of  $P_p = \text{const}$  with increasing  $\sigma_a$  and constant  $\epsilon_r$ , equations (2) and (3) lead to the familiar stress trajectory of a uniaxial strain compaction test:

$$\partial\sigma_r/\partial\sigma_a |_{P_p=\text{const}} = \nu/(1-\nu)$$

For the (unphysical) case of  $K_g \rightarrow \infty$  but finite  $E$  and  $\nu$ , the pore pressure depletion load path is identical [ e.g. we also find that  $\partial(\sigma_r - P_p)/\partial(\sigma_a - P_p)|_{\sigma_a=\text{const}} = \nu/(1-\nu)$  ], and the deformation can be compactly written via definition of effective stresses  $\sigma_{ae} = \sigma_a - P_p$  and  $\sigma_{re} = \sigma_r - P_p$ . However, for the case of finite  $K_g$ , the pore pressure depletion load path follows a systematically different path. This difference results from the fact that in addition to responding to changes in  $\sigma_{ae}$ ,  $\sigma_r$  has to change with decreasing  $P_p$  to counteract the dilation of the grains that results from the reduction in  $P_p$  [e.g. the  $P_p/(3K_g)$  term in equation 3]. The stress trajectory now becomes:

$$\partial(\sigma_{re})/\partial(\sigma_{ae})|_{\sigma_a=\text{const}} = \nu/(1-\nu) + E/(1-\nu)/(3K_g) = 1 - \alpha(1-2\nu)/(1-\nu) \quad (4)$$

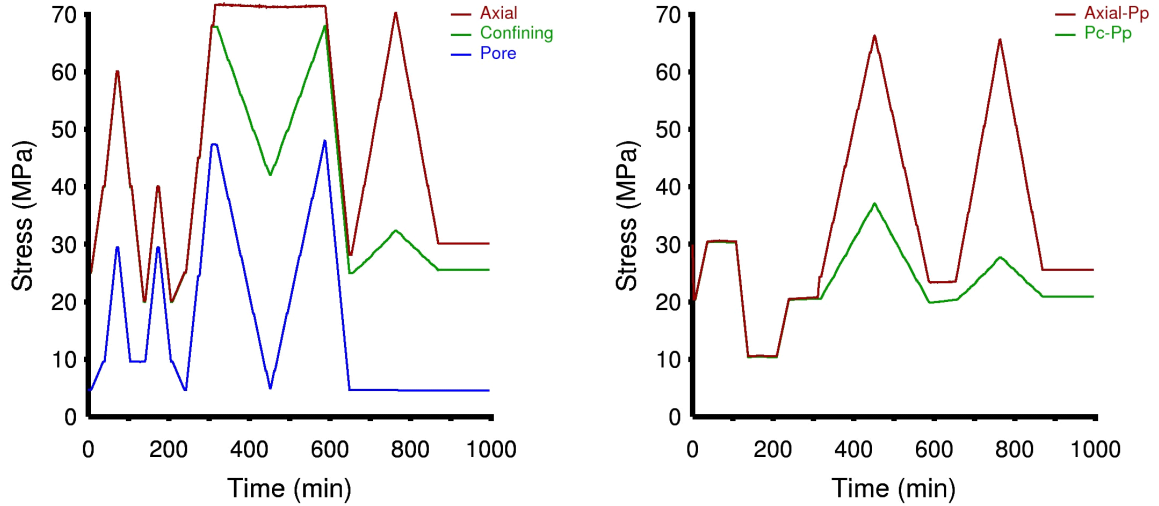


Figure 1: The loading protocol used to examine the difference between pore pressure depletion and constant pore pressure uniaxial strain and their relation to effective stress.

This extra pore pressure effect leads to higher  $\sigma_r - P_p$  and lower  $\sigma_a - \sigma_r$  for a given effective pore pressure depletion  $\sigma_a - P_p$ .

An important point to make here is that the difference between the two loading paths is a function of the elastic constants of the rock and the bulk modulus of the grains. The question now arises as to the possible implications of the differences between the two uniaxial strain loading paths, and whether the concept of effective stress can be used to “correct” experiments using constant pore pressure for applications involving pore pressure depletion.

To help illustrate some issues, we performed an experiment on a homogeneous sandstone plug in a standard rock mechanics test frame. The sample was jacketed in copper foil and instrumented with standard foil strain gages. Corrections were applied for slight pressure effects on the strain gages. The 19% porosity sample was saturated with a mixture of brine and oil. The stress history of the experiment is shown in Figure 1. The initial part of the experiment was designed to measure  $K_b$  (by changing  $P_c$  at constant  $P_p$ ) and  $K_g$  (by changing  $P_c$  and  $P_p$  equally), and thus illustrates how one can constrain and experimentally confirm the concept of a simple effective stress relation in its simplest form. Plotting volumetric strain versus  $P_c - \alpha P_p$ , we find good agreement between data and poroelastic theory (Figure 2).

The second portion of the experiment involves two successive uniaxial strain loading cycles, one using

pore pressure depletion and the other using an increase in axial load at constant pore pressure. One common error is to assume that the  $\alpha$  from (1) can be applied to this loading path as well. Another common error is to assume that  $\alpha$  derived for bulk volume can be applied to other properties (even properties which seem directly related, like pore volume). This is simply not true, even for identical loading paths, a point that is easily derived for the simple case of linear poroelasticity (see Robin [1973] and Zimmerman [2000]).

We use our sandstone experiment to illustrate a number of these points.

*Volumetric Strain Due to Hydrostatic Stresses:* Biot’s classic work leads to the prediction of an effective pressure  $P_e = P_c - \alpha P_p$ , where  $\alpha = 1 - K_b/K_g$ . Using our example sandstone experiment, we find  $K_b = 10$  GPa,  $K_g = 45$  GPa, and thus  $\alpha = 0.78$ . Plotting volumetric strain versus  $P_e = P_c - 0.78P_p$ , we get the result in Figure 2. This confirms the usefulness of the effective stress concept for this case.

*Volumetric Strain Due to Uniaxial Strain Loading:* Through examination of Equations 2 and 3, one can show that for uniaxial strain, the  $\alpha$  derived from hydrostatic loading should apply to the mean stress vs. volumetric strain relationship for uniaxial strain loading. This is confirmed in our experiment (Figure 3), indicating that this sandstone appears to be acting like a

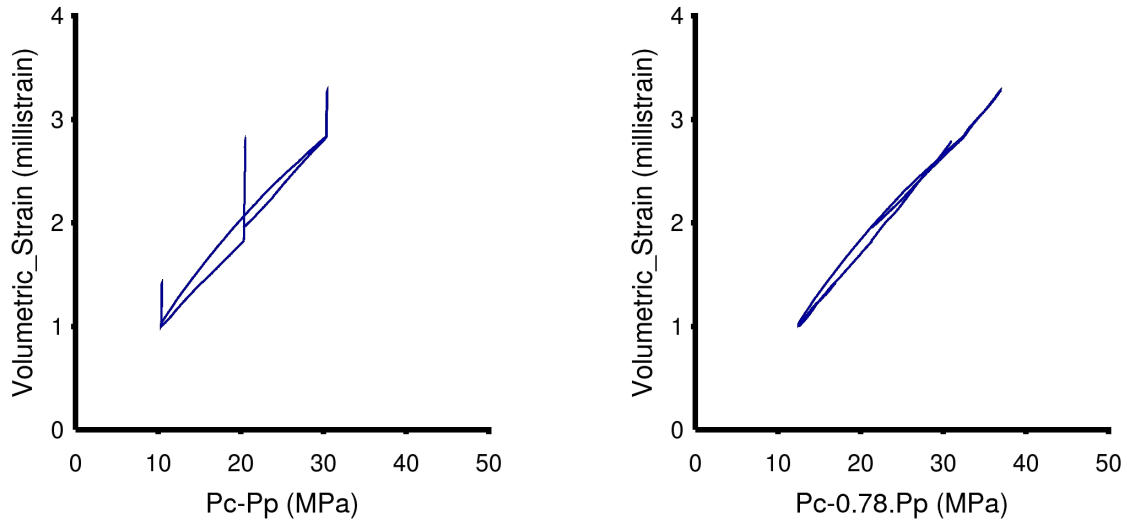


Figure 2: Volumetric strain versus  $P_c - P_p$  and  $P_c - \alpha P_p$  for the hydrostatic portion of the experiment shown in Figure 1.

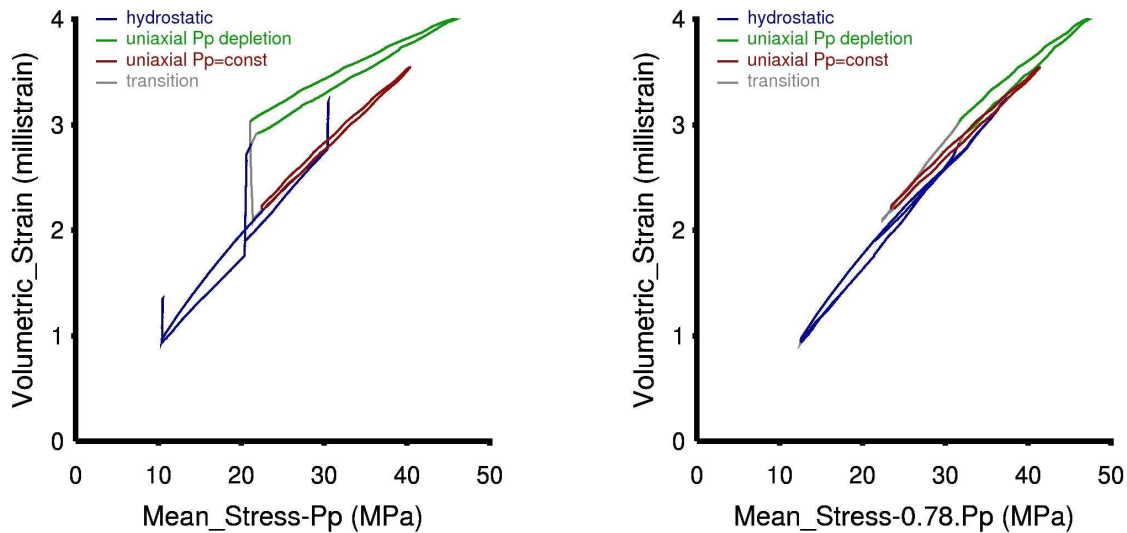


Figure 3: A plot of volumetric strain versus  $\sigma_{\text{mean}} - P_p$  and  $\sigma_{\text{mean}} - \alpha P_p$  using the value of alpha determined from the hydrostatic portion of the experiment (see figure 2). The results indicate that the sample is behaving as a isotropic, linear poroelastic material.

simple isotropic, linear poroelastic material. However, it should be noted that this will only be true for a sample that is linear elastic and isotropic. In reality, rocks such as these can demonstrate both intrinsic and stress induced changes in elastic constants, a case that requires an “ $\alpha$ ” (or set of  $\alpha$ 's) that becomes a function of both loading path and stress.

*Velocity:* It is common to want to apply the concept of effective stress to properties other than elastic deformation. For example, in the case of seismic velocities, one can define an effective stress coefficient ( $\alpha_{vp}$ ) for compressional wave velocity ( $V_p$ ) as:

$$\alpha_{vp} = 1 - [ \partial V_p / \partial P_p |_{P_c-P_p} / \partial V_p / \partial P_c |_{P_p} ]. \quad (5)$$

Measurements of P and S velocities were made during the course of our example sandstone experiment. From the hydrostatic portion, we find that  $V_p$  is best fit by an effective stress relation based on mean stress with  $\alpha_{vp} \sim 0.72$  (Figure 4).

A common error is to assume that  $\alpha_{vp}$  is the same as  $\alpha$  from equation 1. Despite the similarity in value, it should be pointed out that the physical origin of this  $\alpha_{vp}$  is quite different than that for Biot's  $\alpha$ . For example, much of the effect on compressional velocity is predicted by yet another of Biot's theories, that being the theory for wave propagation in a poroelastic solid with finite pore fluid compressibility (Biot [1956]). That theory predicts that

$$V_p = \text{sqrt}[(K_d + 4G_d/3)/\rho] \quad ; \quad V_s = \text{sqrt}[G_d/\rho] \quad (6)$$

where  $K_d = K_b + (1 - K_b/K_g)^2 / [ \phi/K_f + (1 - \phi)/K_g - K_b/K_g^2 ]$  and  $G_d = G$ .

The dependence of both  $K_d$  and  $\rho$  on  $K_f$  leads to a finite value of  $\partial V_p / \partial P_p |_{P_c-P_p}$  and thus a pore pressure effect that can be approximated by an effective pressure relation. Other effects such as changing viscosity and/or fluid compressibility on  $G_d$  (not included in Equation 6) may also play a role, but are not analyzed here. The important point to make is that although  $\alpha_{vp}$  may be coincidentally close to  $\alpha$  for bulk volume, the two  $\alpha$ 's reflect very different physical mechanisms.

It is also noted that the effective stress coefficient for shear wave velocity  $V_s$ , is notably different from that of  $V_p$ . From our data, we find that  $\alpha_{vs} \sim 0.95$  (Figure 5). Here, the physical meaning of  $\alpha_{vs}$  can be understood when one considers  $V_s = \text{sqrt}[G_d/\rho]$  and applying equation 5 but substituting  $V_p$  with  $V_s$ . The dependence of  $\rho$  on  $P_p$  leads to a finite value of  $\partial V_s / \partial P_p |_{P_c-P_p}$ , but

from that effect alone, we should expect  $\alpha_{vs}$  to be slightly greater than 1.0. Experimentally we observe  $\alpha_{vs}$  to be slightly less than 1.0, a fact that we feel is likely caused by fluid viscosity and compressibility stiffening of  $G_d$  causing  $\partial V_s / \partial P_p |_{P_c-P_p}$  to be positive. These same effects would also affect  $\alpha_{vp}$ , reducing  $\alpha_{vp}$  from that predicted by equations 5 and 6. It is a matter of debate as to whether  $\alpha_{vs} < 1$  at seismic and/or borehole acoustic frequencies, where fluid effects on  $G_d$  may be negligible.

Another important point concerning both compressional and shear velocities is that both are sensitive to stress induced anisotropy. While we observe in Figures 4 and 5 that the  $\sigma_{\text{mean}} - \alpha_{vp} P_p$  and  $\sigma_{\text{mean}} - \alpha_{vs} P_p$  do a reasonable job of defining relationships between mean effective stress and  $V_p$  and  $V_s$  for the entire load history, it is clear that during each of the uniaxial strain loadings, the velocities are non-linear functions of  $\sigma_{\text{mean}}$ . This results from the fact that there are other combinations of the stresses that are influencing the velocities, and these relationships are different for  $V_p$  and  $V_s$ .

*Velocity Anisotropy:* For the case of comparing the pore pressure depletion and constant pore pressure loading paths, we find that further considerations are important for reservoir properties that are influenced by the differential axial stress  $\sigma_a - \sigma_r$ . While  $V_p$  and  $V_s$  provide examples where this dependence leads to complications in applying effective stress concepts, velocity anisotropy provides a particularly striking case. Plotting  $V_{ph}/V_{pv}$  versus  $\sigma_a - P_p$  for our sandstone experiment (Figure 6a), we find that under hydrostatic loads, the value of  $P_p$  has no measurable effect on velocity anisotropy in this rock. However, for uniaxial strain, velocity anisotropy changes with  $\sigma_a - P_p$ . In the case of  $V_p$  anisotropy, the change is different for the two uniaxial strain loading paths. In the case of  $V_s$  anisotropy, it is not (Figure 6b). This illustrates the fact that the effects of the differences between pore pressure depletion and constant pore pressure uniaxial strain paths may not always be intuitive. In this case,  $V_p$  anisotropy is a strong function of  $\sigma_a - \sigma_r$ , which is different for a given  $\sigma_a - P_p$  depending on whether  $\sigma_a$  or  $P_p$  are being held constant. In contrast,  $V_s$  anisotropy appears to be a function of a different combination of stresses that happens to be less variable between the two loading paths.

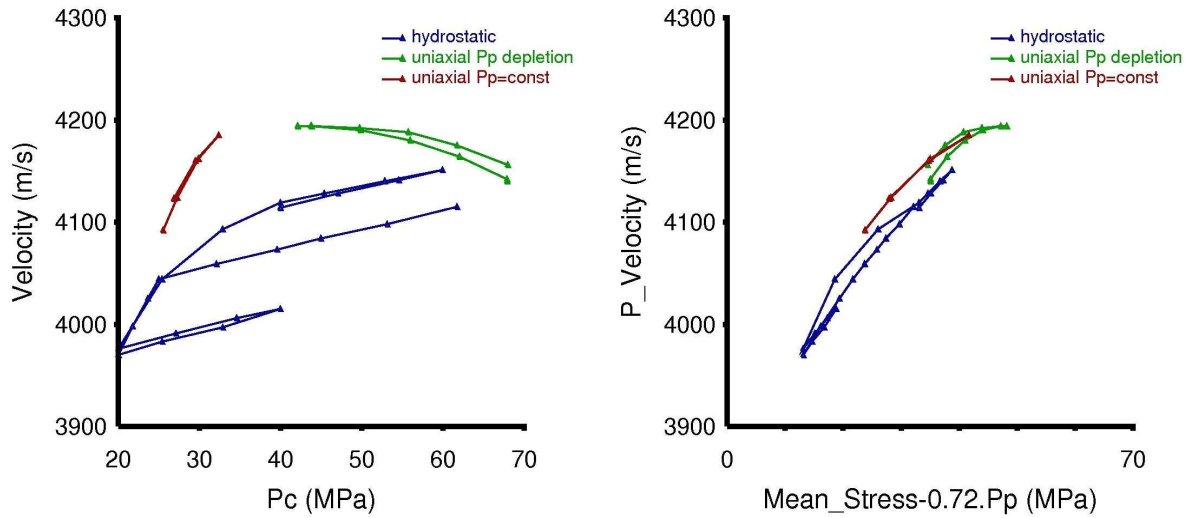


Figure 4: a) A plot of  $V_p$  versus  $P_c$  for the hydrostatic portion of the experiment. A value of  $\alpha_{Vp}$  of 0.72 is determined by application of equation 5. (b) A plot of  $V_p$  versus  $\sigma_{mean}-0.72P_p$  is shown for the entire experiment, indicating how the effective pressure relation determined from hydrostatic portion applies to the uniaxial strain data. Globally the fit is reasonable, but for each of the uniaxial strain loading,  $V_p$  is a different nonlinear function of the  $\sigma_{mean}-0.72P_p$ .

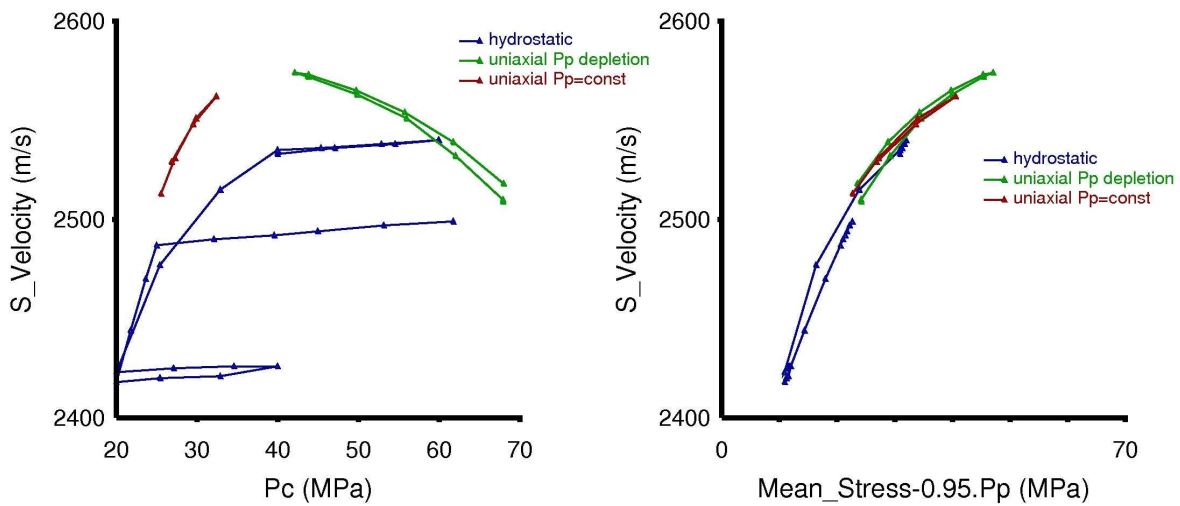


Figure 5: a) A plot of  $V_s$  versus  $P_c$  for the hydrostatic portion of the experiment. A value of  $\alpha_{Vs}$  of 0.95 is determined by application of equation 5. (b) A plot of  $V_s$  versus  $\sigma_{mean}-0.95P_p$  is shown for the entire experiment, indicating how the effective pressure relation determined from hydrostatic portion applies to the uniaxial strain data. Globally the fit is reasonable, but for each of the uniaxial strain loading paths,  $V_s$  is a nonlinear function of the  $\sigma_{mean}-0.95P_p$ .

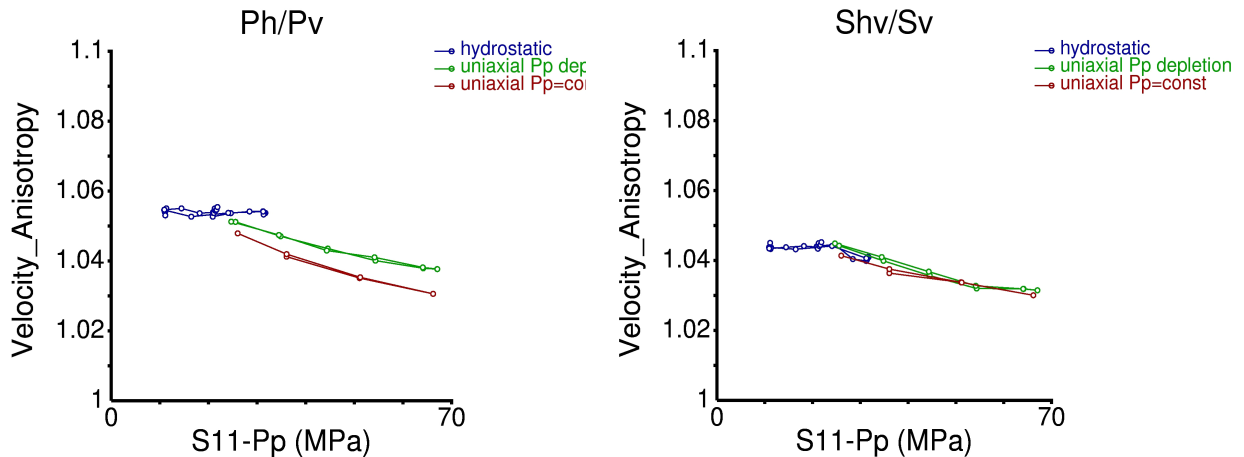


Figure 6: P and S velocity anisotropy versus  $\sigma_a - P_p$ . Ph and Pv refer to the horizontal and vertical P velocity. Shv refers to the vertically polarized horizontal shear velocity, and Sv refers to the vertical shear velocity.

*Additional Measurements of Stress Path and Deformation:* A series of uniaxial-strain compaction experiments was also performed on a set of core samples from a deepwater GoM field. Tests were performed on samples from three different sand units, each unit characterized by porosity in the range 22% - 25%. For each sand, several samples were tested by increasing the axial stress with pore pressure held constant at 500 psi. Then, for each sand, a new sample was tested by holding axial stress constant and reducing pore pressure from ~8000 psi to near zero. Conditions of uniaxial-strain were maintained in all cases. The change in lateral stress was measured during each loading step, as was the sample axial strain.

For all tests, a value of Biot's alpha was calculated using Eqn 1, assuming a grain compressibility of  $1.6E-07$  1/psi and using the equivalent hydrostatic bulk compressibility measured on the sample, defined as volume strain divided by change in mean effective stress (converted to conditions of constant pore pressure if necessary). Poisson's ratio was extracted from the measured change in lateral stress. From the results of the tests with constant pore pressure, an 'expected' magnitude of lateral stress change for the case of constant axial stress can be calculated using Eqn. 4.

The results are compiled in Table 1. For each sand, the average results of the tests with constant pore pressure are used to predict the 'stress path' for a test with constant axial stress,  $\partial(\sigma_r - P_p)/\partial(-P_p)$ . The second row for each sand lists the results directly measured on the test with constant axial stress. The prediction from Eqn. 4 is close, but does not exactly match the measurement. This is likely due to the fact that the samples are responding somewhat non-linearly and with some degree of permanent deformation. In addition, the samples are spaced many feet apart, so each sample is slightly different.

Also included in Table 1 are the measurements of sample bulk volume compressibility. For conditions of uniaxial-strain this is equal to  $\partial(\epsilon_a)/\partial(\sigma_a)$  for constant pore pressure and equal to  $\partial(\epsilon_a)/\partial(-P_p)$  for constant axial stress. In the case of linear poroelasticity, the two quantities are theoretically related by  $\partial(\epsilon_a)/\partial(-P_p) = \alpha[\partial(\epsilon_a)/\partial(\sigma_a)]$  (see Zimmerman 2000).

From the tests with constant pore pressure, an expected value of  $\partial(\epsilon_a)/\partial(-P_p)$  is calculated. Just as for the magnitudes of lateral stress change, it is seen that the values predicted from poroelastic equations do not quite match the values directly measured using constant axial

stress with changing pore pressure, but that linear poroelasticity does a reasonable job of explaining the differences between these two loading paths.

While simple theory can explain elastic deformation, we use this data to illustrate a potential issue. Figure 7a plots the measured change in  $(\sigma_r - P_p)$  vs.  $(\sigma_a - \sigma_r)$  for each of the two test types and for each of the three sands. It is clearly seen that the change in lateral effective stress is less when the pore pressure is held constant, compared to the more realistic case of changing pore pressure. This results in a different stress path.

In some deepwater sands and/or depletion scenarios, we observe the onset of nonlinear compressibility due to pore collapse at high depletions. Since most commonly employed failure criteria can be expressed as a function

of  $\sigma_a - \sigma_r$  and  $\sigma_r - P_p$ , it should be expected that the onset of inelastic deformation will occur at different “effective pore pressure depletions” for the two uniaxial strain loading paths (Figure 7b). Thus, the choice of loading path can have fundamental impact on reservoir engineering decisions. It is issues like these where direct experimentation is required to understand the sensitivity of phenomena such as inelastic deformation and pore collapse to the differences in these loading paths. If the differences are found to be small over the range of stresses expected, then constant pore pressure testing can be used as a substitute for pore pressure depletion. If not, then the pore pressure depletion loading protocol should be used to assure that the most appropriate loading path is used for constraining reservoir models.

Table 1: Results of uniaxial-strain tests using different loading protocols.

Sand	Held constant:	# samples	$\alpha$	$\partial(\sigma_r - P_p)/\partial(\sigma_a)$	$\partial(\sigma_r - P_p)/\partial(-P_p)$	$\partial(\epsilon_a)/\partial(\sigma_a)$ (1/psi)	$\partial(\epsilon_a)/\partial(-P_p)$ (1/psi)
A	$P_p$	4	.861	.193	.305	5.35E-07	4.62E-07
A	$\sigma_a$	1	.870		.280		4.79E-07
B	$P_p$	6	.876	.173	.275	5.82E-07	5.10E-07
B	$\sigma_a$	1	.875		.327		5.47E-07
C	$P_p$	2	.842	.113	.254	4.13E-07	3.48E-07
C	$\sigma_a$	1	.837		.246		3.27E-07

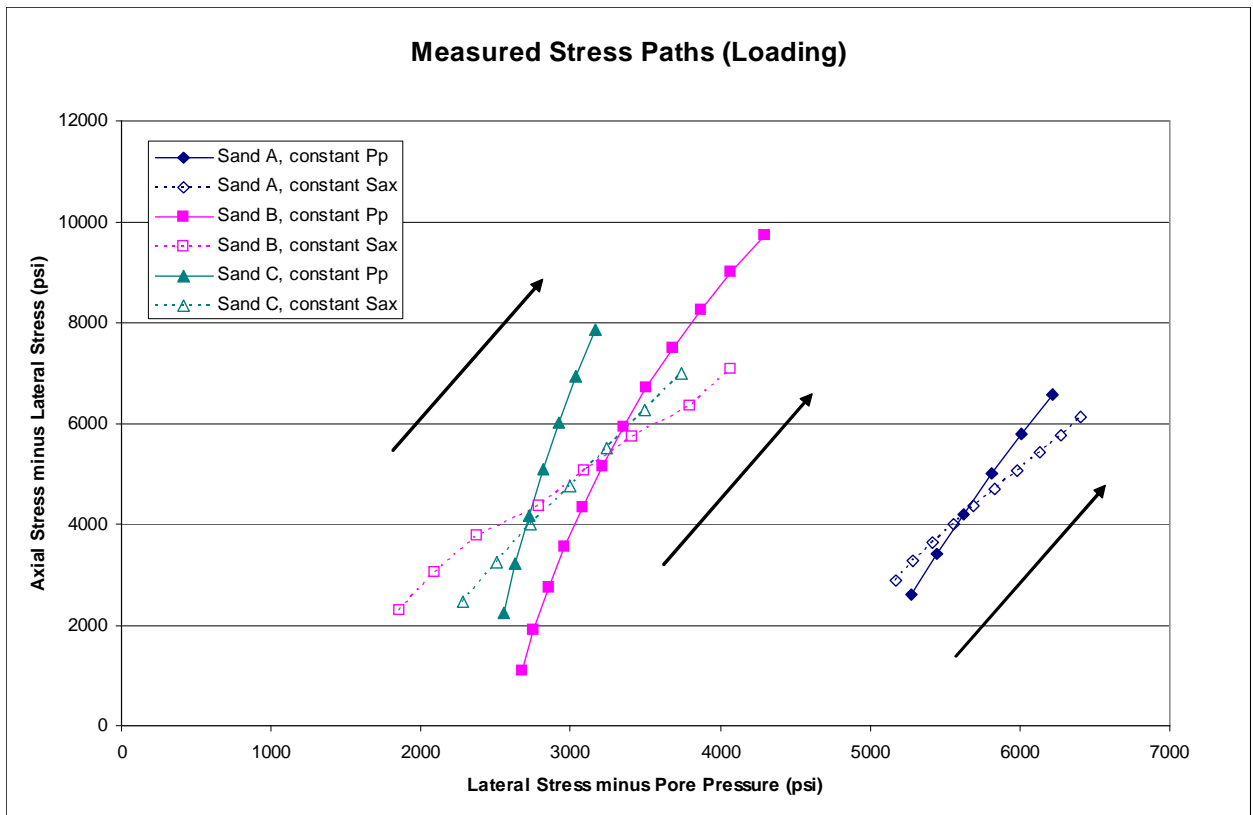


Figure 7a: Measured stress paths with different uniaxial-strain loading protocols, example GoM core.

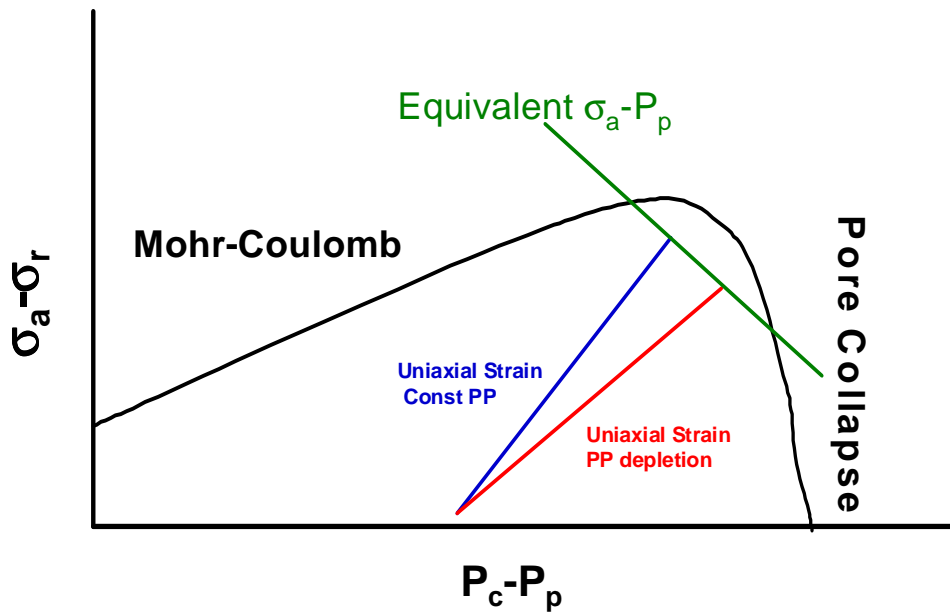


Figure 7b: Illustration of the potential impact of uniaxial strain loading path on predictions of depletion induced inelastic deformation. The two paths intersect the “failure” criterion at different effective depletions ( $\sigma_a - P_p$ )

**EFFECTIVE STRESS FOR PERMEABILITY**

In contrast to many other properties, the effective stress coefficient for permeability is commonly reported to be one or greater. Thus with increasing pore pressure at a constant net confining stress, the permeability may actually increase (e.g. Al-Wardy & Zimmerman, 2004 & Warpinski & Teufel, 1992). The rationale for this is that at high pore pressures, grains that are not part of the load bearing frame work are compressed by the pore pressure, thus effectively increasing the diameter of the pore throats and thereby the permeability; Figure 8.

It is very difficult to obtain measurement of transverse permeability on a vertical plug during a true uniaxial pore pressure depletion. Therefore for this scoping study we have determined the effective stress coefficient during a hydrostatic compaction. Brine saturated samples were mounted in a hydrostatic core holder and the brine permeability was measured by flowing brine at a constant flow rate. Permeability measurements were conducted after 2 to 3 hours at each new pore pressure or confining stress.

There are three possible sets of measurements to study effective stress and brine permeability.

- Test #1. Constant (P<sub>c</sub>-P<sub>p</sub>) with increasing P<sub>p</sub>.
- Test #2. Constant P<sub>p</sub> with increasing P<sub>c</sub>.
- Test #3. Constant P<sub>c</sub> with decreasing P<sub>p</sub> (pore pressure depletion).

In order to calculate an effective stress coefficient for permeability, one needs to conduct at least two sets of these tests, preferably on the same sample. This can be either the combination of tests #1 & #2 (protocol 1) or

tests #2 & #3 (protocol 2).

To illustrate the effect of pore pressure on permeability for deepwater GoM LT sandstones, we present here the results of a scoping study on three core plugs with nominal permeabilities of 0.1, 1, and 10 mD. The permeability data for the ~10 md sample using protocol #1 is presented in Table 2.

In the first set of three permeability measurements, Tests #1, the net or differential stress (P<sub>c</sub>-P<sub>p</sub>) hereafter referred to as NCS is held constant while the pore pressure was increased whereby the brine permeability increased by 18% (Table 1 and Figure 9). In the second set of three permeability measurements, Tests #2, the pore pressure is held constant while the confining pressure was increased whereby the brine permeability decreased by 9%. Using this combination of two sets of measurements, Protocol #1 results in an α<sub>perm</sub> of 2.48 as shown in equation (9) and in Figure 9.

$$\alpha_{perm} = 1 - (\partial k / \partial P_p)_{P_d} / (\partial k / \partial P_d)_{P_p} = 2.48 \tag{9}$$

where k is the permeability and P<sub>d</sub> = P<sub>c</sub>-P<sub>p</sub>. In Table 2, the α<sub>perm</sub> value of 2.48 is used to calculate an “effective stress” and is plotted versus brine permeability ratio in Figure 10. This figure also contains a plot of permeability ratio versus P<sub>c</sub>-P<sub>p</sub> illustrating how the α<sub>perm</sub> of 2.48 collapses the data to a smooth function.

The permeability for this plug at any combination of pore pressure and confining stress can now be expressed by equation (10).

$$k = 1.02 * \text{EXP}(-1.4\text{E-}05 * (P_c - 2.48 * P_p)) \tag{10}$$

Using (10), we can predict permeability during a pore

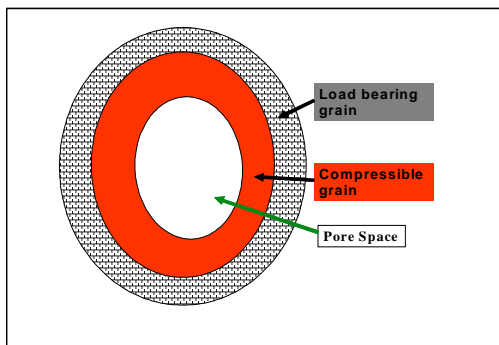


Figure 8: Cross-section of pore throat

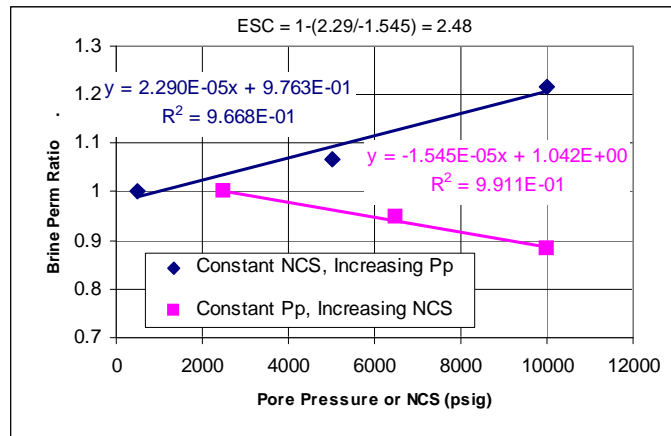


Figure 9: Permeability results using protocol #1 for Sample #1 with Kair > 10 mD.

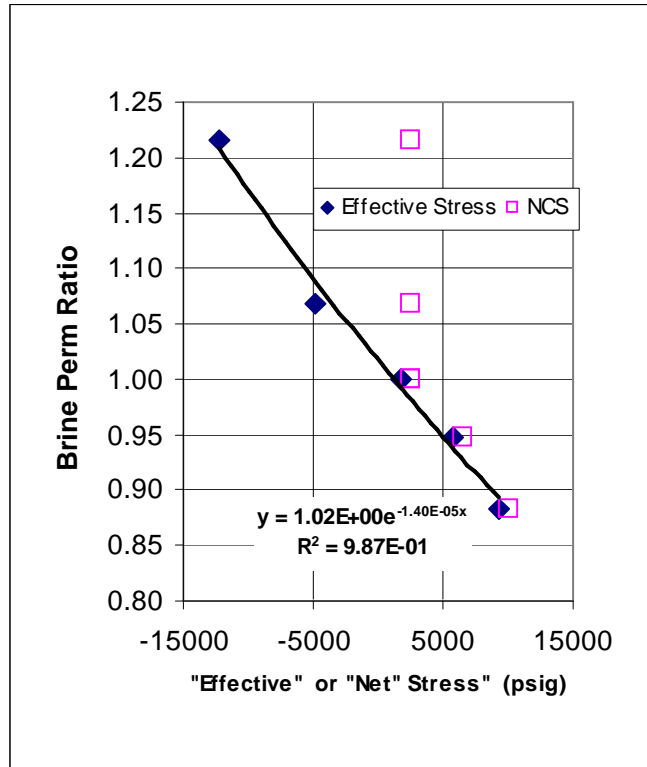


Figure 10: Effective Stress Law for Perm for sample #1

Table 2: Effective Stress Law for Permeability				
Net Confining Stress psig	Confining Stress psig	Pore Pressure psig	"Effective Stress" $\alpha_{perm} = 2.48$	Perm ratio
2,500	3,000	500	1,760	1.00
2,500	7,500	5,000	-4,900	1.07
2,500	12,500	10,000	-12,300	1.18
2,500	3,000	500	1,760	1.00
6,500	7,000	500	5,760	0.94
10,000	10,500	500	9,260	0.91

Table 3: Predicted Permeability for Pore Pressure Depletion				
Confining Stress psig	Pore Pressure psig	"Effective Stress" $\alpha_{perm} = 2.48$	Perm ratio #1	Perm ratio #2
22500	20000	-27100	1.48	1.00
22500	18000	-22140	1.38	0.93
22500	16000	-17180	1.29	0.87
22500	14000	-12220	1.20	0.81
22500	12000	-7260	1.12	0.76
22500	10000	-2300	1.05	0.71
22500	8000	2660	0.98	0.66

pressure depletion test at constant confining stress and decreasing pore pressure (Test #3 of the three possible combinations of pore pressure and confining stress). Predictions are shown in Table 3 and in Figure 11.

Equation (10) predicts that maintaining a constant differential stress of 2500 psi while increasing the pore pressure from 10,000 psi to 20,000 psi will increase the initial permeability ratio from 1.18 to 1.48 (Perm ratio #1, where the ratio is normalized to 1.0 at  $P_d = 2,500$  psi and  $P_p = 500$  psi). In Table 3, the column Perm Ratio #2 is the permeability normalized to the initial predicted permeability at  $P_d = 2,500$  psi and  $P_p = 22,500$  psi.

Figures 12 and 13 provide similar plots as Figure 11 for samples in other permeability ranges. We have found with brine permeability measurements on core samples that the permeability increase is an exponential function of the pore pressure, thus with pore pressures less than 5,000 psi the increase is less than 5% and would be considered within the noise/uncertainty of the permeability measurement. At a pore pressure of 10,000 psi the % increase in permeability over that at 500 psi, has increased by 5% to 25% with a projected increase by 20,000 psi of 10 to 50%.

What is the impact of this effect of pore pressure on permeability? The main permeability characterization of reservoir rock is based on the air permeability measured on the core plugs at one per foot. These air permeability measurements are conducted at low pore pressures (usually 10's to a few 100's psi mean pore pressure). Even when brine permeabilities are obtained to compare with air permeability, they are typically done at low backpressure (e.g. less than 1000 psi). The pore pressure used in oil perm at connate water saturation may depend on whether live or dead oil is used, but typically the pore pressures would be less than 5,000 psi if only for sake of convenience. Thus all of these permeability measurements are likely to significantly understate the in-situ reservoir permeability when pore pressures are in the 20,000+ psi range.

The bias of routine core analysis air permeability is offset by the fact that as the reservoir is being produced, the pore pressure decreases, which will result in lower permeabilities because of the effective stress law. Also pore pressure depletion will result in a permeability reduction simply because of the increase in the net

confining stress. Thus now there are two mechanisms that will result in lower permeability during pore pressure depletion: (1) increasing net confining stresses (reducing pore throat size) and (2) decreasing pore pressure (increasing volume of grains within pores). From the results shown in Figures 11 to 13 the decreasing pore pressure has a greater impact on permeability than the increasing differential stress.

Currently most US core analysis services companies are not equipped to measure transverse permeability on a vertical core plug during uniaxial compaction, simulating reservoir stress-strain at reservoir conditions of stresses, pore pressures, and temperature. Therefore we are unable to obtain these data directly. Another issue that is raised is that if high pore pressure enhances the absolute brine permeability, what impact will high pore pressure have on relative-permeability and capillary pressure?

*Protocol Comments:* We need to be careful of how hysteresis (permanent permeability loss or change) could alter the test results and conclusions.

We feel that it is preferable to start with Test#1 and to combine all three possible tests, Test #1, Test #2, and Test #3 into one testing sequence as the following.

1 - 2 - 2 - 3 or 1 - 3 - 3 - 2

The reason for repeating the middle load sequence is that the second load sequence could cause some permanent change to the permeability. But from then on everything should be repeatable. So the third and fourth sequences can then be directly compared, which when combined with the #1 loading gives more complete information on the behavior of the sample and on the effective stress law, not to mention data redundancy.

The following loading sequence 1-3-3-2 shown in Figure 14 is currently under investigation, having been chosen because Test #1 brings the sample pretty much back to in situ conditions, and Test #3 is a direct simulation of what will happen when the reservoir first sees pressure depletion occurring. Therefore the data become even more applicable to field planning.

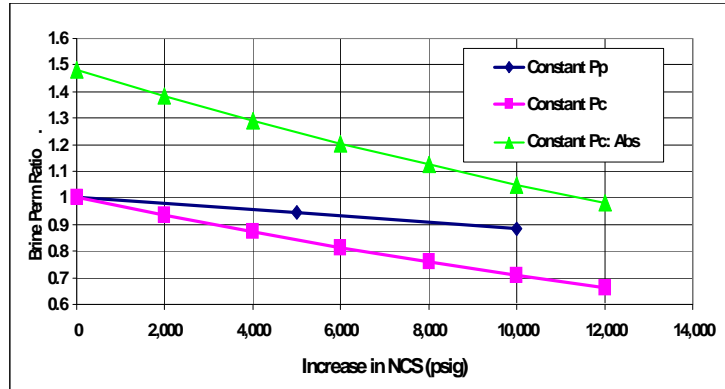


Figure 11: Predicted effect of increasing stress on permeability for Sample #1

**Legend for Figures 11 - 13**  
 Curve: Constant Pc = Pore Pressure Depletion (color = magenta)  
 Initial Hydrostatic conditions: Pc = 22,250 psi;  
 Pp = 20,000 psi  
 Pp is decreased by 12,000 psi;  
 perm ratio basis is initial perm at initial conditions, Pp = 20,000psi

Curve: Constant Pc (Abs) = Pore Pressure Depletion (color = green)  
 Initial Hydrostatic conditions: Pc = 22,250 psi;  
 Pp = 20,000 psi  
 Pp is decreased by 12,000 psi;  
 perm ratio basis is initial perm at Pp = 500 psi

Curve: Constant Pp = Constant Pore Pressure (color = navy blue)  
 Initial Hydrostatic conditions: Pc = 3,000 psi;  
 Pp = 500 psi  
 Pc is increased by 10,000 psi;  
 perm ratio basis is initial perm at Pp = 500 psi

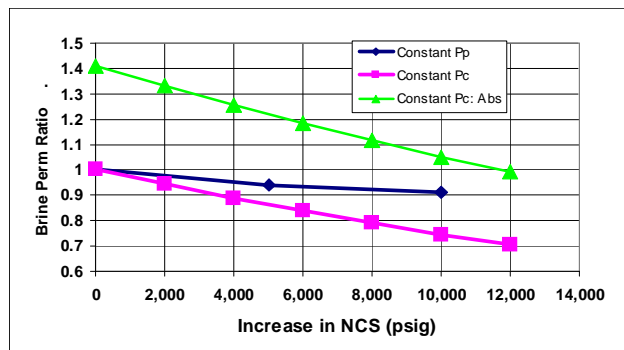


Figure 12: Sample #2 with K<sub>air</sub> > 1 mD & < 10 mD and α<sub>perm</sub> = 2.58

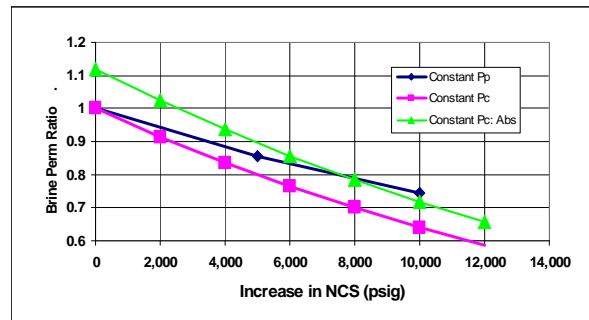


Figure 13: Sample #3 with K<sub>air</sub> < 1 mD and α<sub>perm</sub> = 1.16

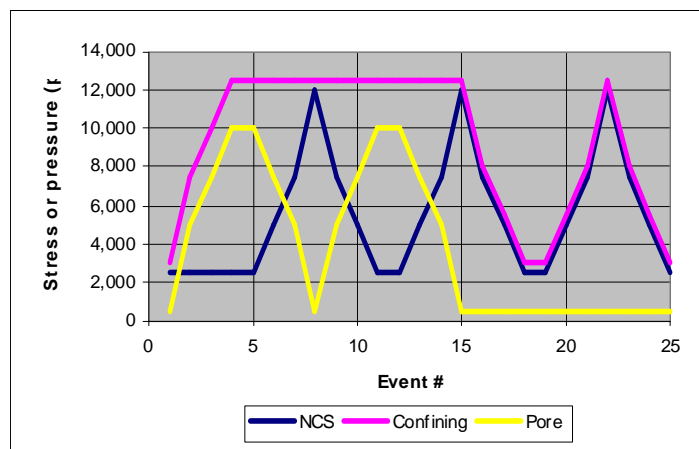


Figure 14: Pore pressure and confining stress for protocol 1-3-3-2

## CONCLUSIONS

- Stress-strain paths for constant pore pressure and pore pressure depletion are potentially different thus complicating mapping effective stress to pore pressure depletion response.
- Effective stress coefficients can be (and usually are) different for different properties.
- The effective stress should not be considered as an equivalent state of stress.
- Whenever possible, true pore pressure depletion tests are preferred.
- Routine core analysis permeability measurements at low pore pressure may significantly underestimate permeability at reservoir pore pressures.
- Transverse permeability measured during uniaxial pore volume compressibility tests at constant pore pressures may underestimate permeability reduction during pore pressure depletion tests.
- Core analysis and rock mechanics service company laboratories should acquire capability to conduct tests at reservoir pressures and stresses.

## ACKNOWLEDGEMENTS:

We thank Reservoir Management Group, NER, and Chevron for their support and approval to publish this paper. We thank James Noel for assistance in performing the example sandstone experiment, and Craig Bovberg for assistance with the field-core uniaxial-strain tests.

## REFERENCES

- Al-wardy, W. and Zimmerman, R.W., 2004, "The Effective stress law for the permeability of clay-rich sandstones", *J. of Geophy. Res.*, 109, B04203, 10 pages.
- Biot, M.A. 1956, Theory of propagation of elastic waves propagation in a fluid saturated porous solid I. Low frequency Range, *J. Acoust. Soc. Am.*, 28, 168-191.
- Biot, M. A. 1962, Mechanics of deformation and acoustic propagation in porous media, *J. Appl. Phys.*, 33, 1482-1498.
- Hofmann, r., Xiaoxia, X., and Batzle, M., 2005, "Effective pressure or what is the effect of pressure?", *The Leading Edge*, Dec., 1256-1260.
- Katahara, K., 2005, "Selecting which stress to use in velocity stress models for pressure estimation", SEG Conference in Houston , 4p.
- Keaney, G., Meredith, P., Murrell, S., and Barker, J., Determination of the Effective Strss Laws for Permeability and Specific Storage in a low Porosity Sandstone, Gulf Rocks 2004, the Proc. 6th North America Rock Mechanics Symposium (NARMS), June 5 - 9, 2004 , Houston, Texas #ARMA/NARMS 04-534
- Klimentos, T., Harouaka, A., Mtawaa, B., and Sanar, S., 1998, "Experimental Determination of the Biot Elastic Constant: Applications in Formation Evaluation (Sonic Porosity, Rock Strength, Earth Stresses, and Sanding Predictions), *SPE Res. Eval & Eng.*, Feb, pp57-63.
- Mese, A., 2005, "Pore Pressure Effect on Mechanical and Acoustic Properties in Shale and Sand" SEG Conference in Houston , 4p.
- Robin, P., 1973, "Note on Effective Pressure, Jr. of Geophysical Research, 78, #14, pp2434-2437.
- Shafer, J. and Fate, T., 2007, "Coring and Core Analysis: Challenges Of Offshore Ultra Deep Water Reservoirs", International Symposium of the Society of Core Analysts, Calgary, Canada, September 08-13, 2007SCA-21.
- Skomedal, E., Jostad,H., and Hettema, M., 2002, "Effective of pore pressue and strsss path on rock mechanical properties for HPHT Application" SPE/ISRM 78152, Rock Mechanics Conference, Irving, Texax, Oct. 20-23, p 10.
- Warpinski, N.R., and Teufel, L.W., 1992, "Determination of the Effective Stress Law for Permeability and Deformation in Low-Permeability Rocks," SPE Formation Evaluation, June, 123-131.
- Worthington, Paul F., Daines, Jeremy M., Bratli, Rolf K., and Nicolaysen, Rune, 1997, "Comparative Evaluation of Core Compaction Corrections for Clastic Reservoir", *The Log Analyst*, Sept-Oct, 19-29.
- Zimmerman, R., 2000, Implications of Static Poroelasticity for Reservoir Compaction, Proc. 4<sup>th</sup> North Amer. Rock Mech. Symp., A.A. Balkema, Rotterdam, pp. 169-72.

## ABOUT THE AUTHORS

John L. Shafer has been a consultant to Reservoir Management Group for the past nine years since retiring from Exxon after 19 nineteen years. For the past five years he has been a consultant to Devon Energy's Gulf Division. Quantification of reservoir quality with low field NMR, core image analysis, and petrology has been the focus of his research. He is a past President of the Society of Core Analysts (SCA), a chapter of SPWLA. John obtained a B.S. in Chemistry from Allegheny College in 1963, his Ph.D. in chemistry from University of California, Berkeley in 1970, and a M.S. degree in petroleum engineering from the University of Houston in 1992.

Greg N. Boitnott is Vice President of New England Research Inc. He specializes in core measurements and analysis with an emphasis on the development of physical models. Areas of current interest include petrophysical upscaling and core to log integration. Greg received a B.S. in Geology from Beloit College, and a Ph.D. in Rock Mechanics from Columbia University in New York.

Russell T. Ewy is a Senior Staff Research Scientist with Chevron Energy Technology Co., where he performs research and technical service in the areas of reservoir and wellbore geomechanics. Prior to joining Chevron in 1996 he was with Exxon Production Research Co. for seven years. Russ has served on the Board and the Executive Committee of the American Rock Mechanics Association, and is currently a review chair for the SPE Journal. Russ has a B.S. and M. Eng. in Mineral Engineering, and a Ph.D. in Rock Mechanics, all from the University of California at Berkeley.